ZTEM™ AIRBORNE AFMAG EM AND GROUND GEOPHYSICAL SURVEY COMPARISONS OVER THE PAMPA LIRIMA GEOTHERMAL FIELD IN NORTHERN CHILE

PRESENTED AT GRC AND SEG 2013

Jean M. Legault
Geotech Ltd.
jean@geotech.ca

Silvia Lombardo
Geotech Ltda. S.A.
silvia@geotech.ca

Shengkai Zhao
Geotech Ltd.
shengkai@geotech.ca

Jorge Clavero
Energia Andina S.A.
jclavero@Energiandina.cl

Igor Aquirre
Energia Andina S.A.
iaguirre@Energiandina.cl

Rodrigo Acros
Energia Andina S.A.
rarcos@Energiandina.cl

Elias Lira
Energia Andina S.A.
elira@Energiandina.cl

SUMMARY

A ZTEM™ (Z Tipper Axis Electromagnetic) airborne AFMAG survey was conducted over the Pampa Lirima geothermal project where a number of other ground geophysical surveys had been previously undertaken, including magnetotelluric (MT), time domain transient electro-magnetic (TDEM), and DC resistivity soundings. Resistivity methods such as MT are typically used to map structure, lithology and alteration, especially the low resistivity cap over the outer margins of the geothermal reservoir at depth. The ZTEM survey at Pampa Lirima overflew the area for comparison purposes.

The ZTEM results appear to correlate well with previous geophysics and the known geology, including known fault structures and contacts, as well as a prominent conductivity high over the Lirima hot spring field. 2D inversions of the airborne ZTEM appear to agree quite well with 3D inversion of ground MT for shallower depths (<2km), in particular the conductive clay-cap attributed to the deep 3D MT conductive heat source and a resistive NE-SW lineament that extends between the Lirima and San Andrés hot springs. Joint 3D MT-ZTEM inversion results should improve the accuracy and the areal extent of the known subsurface resistivity structure at Pampa Lirima.

Key words: Airborne, AFMAG, Chile, electromagnetic, geophysics, inversion, magnetotelluric, resistivity, ZTEM

INTRODUCTION

A ZTEM (Z-Tipper Axis Electromagnetic; Lo and Zang, 2008) airborne AFMAG survey was conducted over the Pampa Lirima geothermal prospect in northern Chile (Figure 1) in December, 2010. Resistivity and EM methods are used in geothermal exploration to map the electric properties of the geology at depth. However, while these preferred methods, like ground magnetotellurics (MT), provide excellent depths of investigation and resolution, they come at a very high cost.

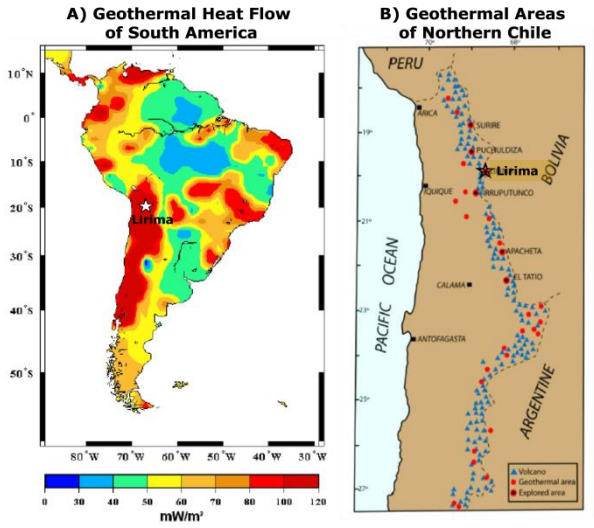

Figure 1: Showing Pampa Lirima in: a) geothermal heat flow map of South America; and b) geothermal areas of Northern Chile (after Haraldsson, 2012).

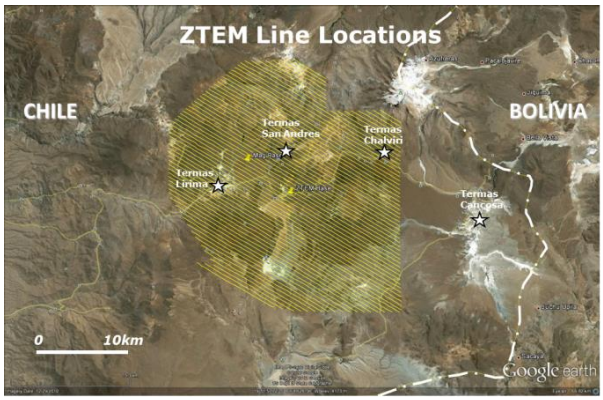

Figure 2: Google Earth image showing ZTEM line – locations and known geothermal prospects at Pampa Lirima.

ZTEM is an airborne variant of the tipper AFMAG method (Ward, 1959; Labson et al., 1985) and is a relatively new air-borne technology for geothermal exploration that is capable of mapping the electrical properties of large areas, in conjunction with MT (Legault et al., 2010; Lazaro et al.,

2011; Legault et al., 2011), to reasonably great depth (>1km), at a fractional cost of ground geophysical methods. The ZTEM survey was flown to test its capability as a reconnaissance resistivity map-ping tool and in direct comparison with magnetotelluric and other ground geophysical results.

The Pampa Lirima project area (Arcos et al., 2011), belonging to Energía Andina, a Chilean geothermal energy company, is located in the Altiplano of northern Chile, approximately 1700 km north of Santiago, near the Bolivian border, in a region of high heat flow and known geothermal prospectivity (Figure 1). Pampa Lirima is long well known for its hot springs and several known geothermal occurrences lie within the survey area, including Termas Lirima to the west, Baños San Andrés further northeast and Baños Chalviri to the northeast, as well as Termas Cancosa, southeast of the property (Figure 2).

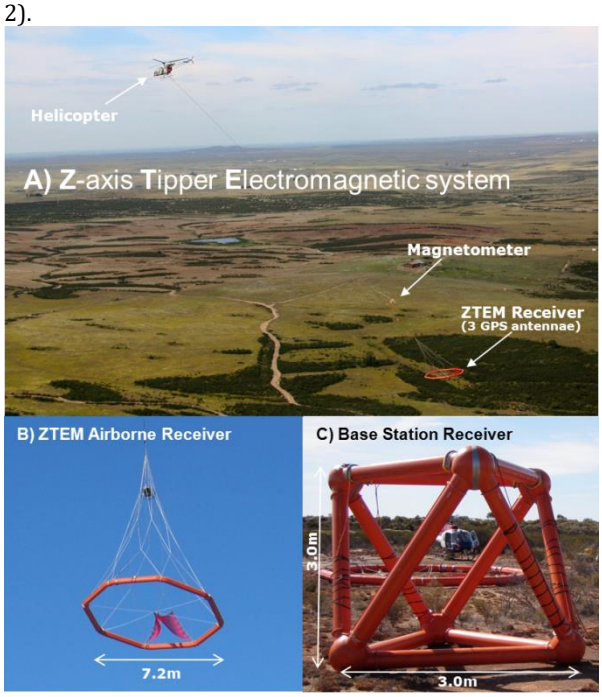

Figure 3: a) ZTEM helicopter EM system in flight, showing HZ receiver Coil and magnetic sensor; b) Hz receiver coil, c) Hx-Hy base station coils located at a remote site adjacent to survey area.

The Pampa Lirima ZTEM survey consisted of 1630 line-km over a 675km2 area using the helicopter-towed ZTEM system (Figure 3), as well as combined aeromagnetics. The survey consisted of 18-95 km long, N-120O oriented flight lines obtained at nominal 425m line spacings. Z-axis tipper measurements of the vertical (Z) component were obtained using an induction aircoil sensor, suspended at approximately 90m elevation above ground level. The vertical component time-series data (Hz) were acquired at 2k Hz, then merged with similarly sampled horizontal field measurements (Hx-Hy) from fixed base-station reference coils, in order to obtain the tipper vectors Tzx (in-line) and Tzy (cross-line). The ZTEM tipper In-Phase and Quadrature transfer functions were derived from 1.0sec time-series using Fourier-based, digital signal processing analyses, and then were output at 2.5Hz (~10m stations) for 6 frequencies, between 25Hz and 600Hz. The magnetometer was an optically pumped caesium vapour magnetic field sensor, towed at approximately 20m above the ZTEM sensor, roughly at 110m ground elevation.

GENERAL THEORY

The ZTEM airborne AFMAG system measures the anomalous vertical secondary magnetic fields that are created by the interaction between naturally occurring, plane wave audio frequency EM fields and electrical heterogeneities in the earth. The vertical magnetic field (**Hz**) is linearly related to the horizontal fields (**Hx**, **Hy**) according to the following (Vozoff, 1972):

$$\mathbf{Hz = Tzx\ Hx + Tzy\ Hy} \qquad (1)$$

where the magnetic field vector T = (Tzx, Tzy), known as the tipper, is complex and a function of frequency, but has rotationally invariant properties, such as its magnitude and direction, that are independent of the subsurface, the measurement direction and the field polarization (Labson et al., 1985).

AFMAG uses naturally occurring audio frequency magnetic fields from worldwide atmospheric thunderstorm activity as the source of the primary field signal, and therefore requires no transmitter (Ward, 1959). The primary fields resemble those from VLF except that they are not man-made, are at lower frequency (tens & hundreds of Hz versus tens of kHz), are pseudo-random rather than cyclically repetitive, and are usually not as strongly directionally polarized. The EM fields used in AFMAG have the unique characteristic of being uniform, planar and horizontal, and also propagate vertically into the earth, to great depth, up to several km, as determined by the magnetotelluric (MT) skin depth (Vozoff, 1972):

$$\mathbf{\delta_S = 503 * \sqrt{(\rho / f)}\ metres} \qquad (2)$$

where $\boldsymbol{\rho}$ is the bedrock resistivity (ohm-metres), $\mathbf{f}$ is the frequency of measurement (hertz) and $\boldsymbol{\delta_S}$ is the depth where the amplitudes of the EM fields are reduced to 1/e (37%) of their surface values. A reasonable rule of thumb estimate for the depth of investigation for MT is taken to be approximately equal to 1.5 skin depths (Spies, 1989).

The tipper from a single site contains information on the dimensionality of the subsurface (Pedersen, 1998), for example, in a horizontally stratified or 1D earth, T=0 and as such Hz is absent. For a 2D earth with the y-axis along strike, Tzy=0 and Hz = Tzx*Hx. In 3D earths, both Tzx and Tzy will be non-zero. Hz is therefore only present as a secondary field due to a lateral resistivity contrast, whereas the horizontal Hx and Hy fields are a mixture of secondary and primary fields (Stodt et al., 1981). But, as an approximation, as in the telluric-magnetotelluric method (T-MT; Hermance and Thayer, 1975), the horizontal fields are assumed to be practically uniform, which is particularly useful for rapid reconnaissance mapping purposes.

By measuring the vertical magnetic field Hz, using a mobile receiver (r) and the orthogonal horizontal Hx and Hy fields at a fixed base station reference site (r0), ZTEM is a direct adap-tation of the T-MT technique for airborne AFMAG surveying. For ZTEM the tipper equation (1) is then rewritten as follows (Holtham and Oldenburg, 2010):

$$\mathbf{Hz(r) = Tzx(r,r_0)\ Hx(r_0) + Tzy(r,r_0)\ Hy(r_0)} \qquad (3)$$

GEOLOGIC SETTING

The geology of the Pampa Lirima prospect (Figure 4) consists of: a) basement Mesozoic carbonate rocks that form a folded and thrusted belt and Cretaceous volcanics that cover the older sediments in angular unconformity; b) Oligocene-Miocene volcanic and sedimentary cover rocks are 500-700m thick and strongly folded; c) covering these rocks are middle-Miocene to Pleistocene volcanic edifices, that form the mountain peaks, reaching to great altitudes and featuring varying degrees of erosion, with large volumes of accumulated material. Struc-turally, a series of NS, NW and NE oriented structures affect the Oligo-Miocene cover rocks as well as the Mesozoic base-ment (Arcos et al., 2011).

The Pampa Lirima survey area is distinguished by its many sectors with distinct colour anomalies (see Figure 2), due to hydrothermal alteration and iron oxide staining. The alteration styles range from argillic (illite-smectite), phyllic (illite-sericite-muscovite) and advanced argillic (silica-alunite-kaolinite). At San Andrés, the alteration is covered by relatively fresh Miocene lavas, unaltered Pliocene volcanics and locally by till deposits. At Lirima, the altered rocks that extend over a large area are gradationally covered by unaltered to altered Miocene lavas (Arcos et al., 2011).

Geologically, the Lirima and San Andrés geothermal systems, which are in the Coscaya River basin and its tributary, both lie along the same NE-SW alignment (Figure 4) and each is asso-ciated with large areas of steam-heated type argillic to advanced argillic hydrothermal alteration. The Chalviri geothermal hot springs (Figure 4), which drain into the Cancosa Basin further southeast, are located in a NW-SE lineament that marks the contact between upper Miocene volcanic complex and the large Pleistocene volcanic edifice of Cerro Sillajhuay to the north (Arcos et al., 2011).

PREVIOUS GEOPHYSICS

The Pampa Lirima geothermal prospect has been host to a number of geophysical surveys, including regional airborne magnetics across the entire property, micro seismic and magnetotelluric coverage spanning the Lirima and San Andrés area (Arcos et al., 2011), as well as individual lines of vertical electrical resistivity soundings (VES) and time-domain EM (TDEM) sounding directly across the Lirima and San Andrés fields (I. Aguirre, pers. comm., 02-2011).

The regional aeromagnetics defined an area of high magnetism at San Andrés that is related to the Miocene-Pliocene volcanic cover. In contrast, Lirima is situated in a large region of low magnetism, reflecting either demagnetized or weakly magnetized rocks, due to hydrothermal alteration. Also, a clear NE-SW lineament joins San Andrés to Lirima (see Figure 4) and appears to coincide with regional structural trends (Arcos et al., 2011).

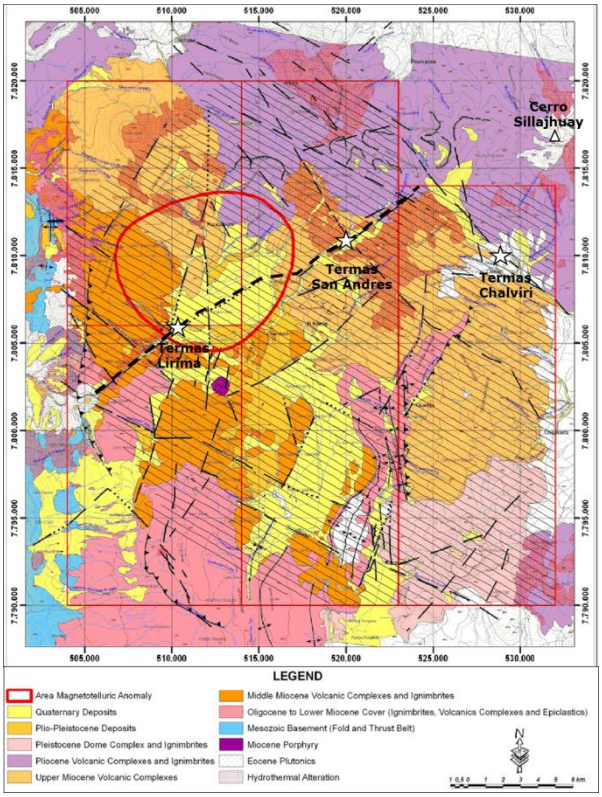

Figure 4: Geological map of Lirima area, with property boundary (red polygons), ground MT deep conductive anomaly (red circle), interpreted major lineament (black dashes) and ZTEM flight (grey lines) lines (after Arcos et al., 2011).

Shallow time-domain electromagnetic (TDEM) soundings using a NanoTEM instrument were obtained at Pampa Lirima (Geodatos, 2010), including two northwest-southeast profiles over the Lirima and San Andrés fields that are presented in Figure 5. 1D inversions for both areas indicate higher resistivities at surface and generally lower resistivities below 100-200m depths, which is consistent with the younger unaltered cover above the more heavily altered basement rocks. At Lirima, anomalous conductivities are detected directly above the hot spring and the inferred NE-SW structure in both TDEM and vertical electrical array sounding (VES) results (see Figure 5 and Figure 6; I. Aguirre, pers. comm.., 02-2011).

The micro-seismic survey that continuously recorded a network of stations at Lirima over a six month period recorded >3500 events, of which 1200 were focused at less than 25km depth. Some of these seismic events tended to be aligned along the MT and aeromagnetic lineament, thereby reinforcing the idea of a major NE-SW structural control (Arcos et al., 2011).

An 82 site full tensor MT survey, consisting of 0.003-10k Hz frequency soundings, was conducted in the Lirima-San Andrés region. These results were then fed to a 3D inversion, using the Mackie and Madden (1993) code for further interpretation (Arcos et al., 2011).

The 3D inversion results (Figure 7) indicate that the south to southwestern survey area is underlain by a shallow conductive layer (<10 ohm-m) within 1000m below the surface, that is interpreted as the clay cap (argillic alteration) of the geothermal reservoir. This clay cap conductive layer is in turn interrupted in the center by a higher resistivity zone (see Figure 7b) that coincides with

the regional NE-SW lineament interpreted from the regional geology and aeromagnetic data.

More importantly, in the southwestern corner of the survey area, below the upper clay-cap conductive layer, a very large (8x8x2km thick) distinctive, deep conductive body is observed at >2km depths. A massive, partially melted intrusive body is given as a possible explanation for this anomaly, which is interpreted to be the heat source for the geothermal system. This would distinguish Pampas Lirima from more typical active volcanic systems that are the heat sources elsewhere in the Andean environment and whose heat sources are usually deep resistive bodies (Arcos et al., 2011).

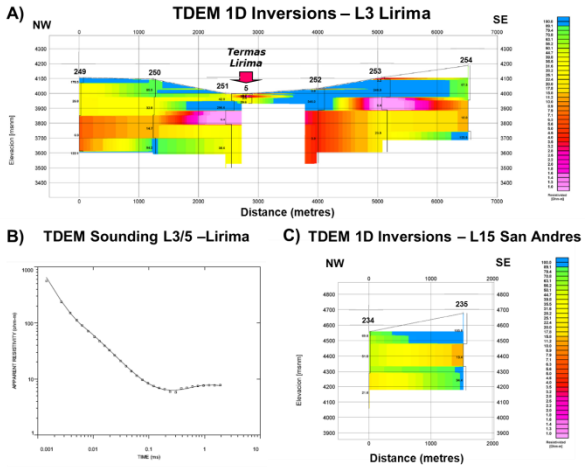

Figure 5: NanoTEM time-domain EM sounding results at Pampa Lirima (Geodatos, 2010): 1d inversion section across Lirima, b) TEM sounding at Lirima, and c) 1D inversion section at San Andrés (after I. Aguirre, pers. Comm., 02-2011). TEM line locations are shown in Figure 6.

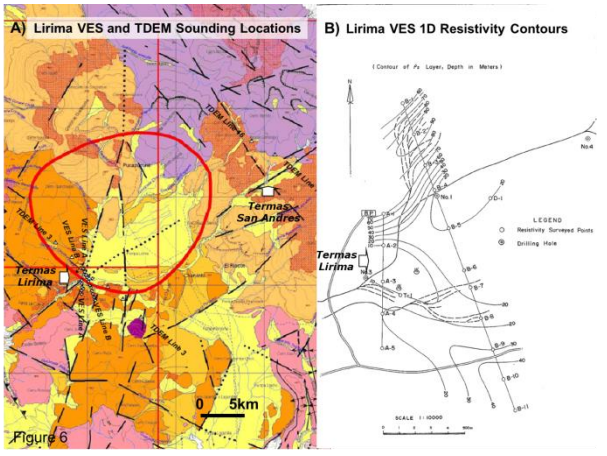

Figure 6: a) VES soundings (circles) and TDEM soundings (triangles) overlain on Lirima geology; b) VES survey (JICA, 1978) 1D resistivity contours for upper layer at Lirima (after I. Aguirre, pers.comm., 02-2011).

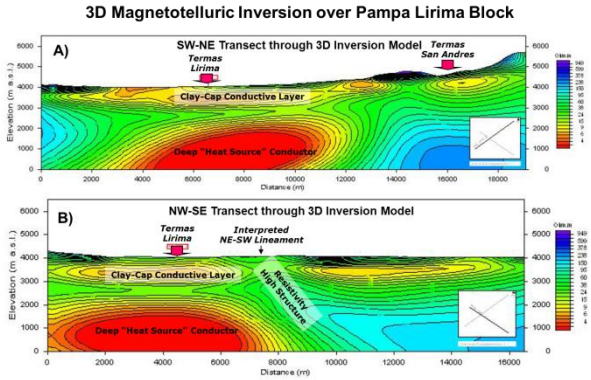

Figure 7: 3D Magnetotelluric inversion results, showing: a) NE-SW and b) NW-SE oriented sections across the 3D model (after Arcos ET AL., 2011). Their location is approximately by the 2D ZTEM inversion lines presented in Figure 8.

RESULTS AND DISCUSSION

Tipper AFMAG data, by their nature, typically exhibit cross-over behaviour over lateral heterogeneities (Ward, 1959; Lab-son et al., 1985). The In-Phase (IP) Total Phase Rotation (TPR) results, shown in Figure 8 and Figure 9, are representations of the ZTEM tipper data that convert cross-overs to single-peak responses while allowing the orthogonal Tzx and Tzy components to be combined. Analogous to the DT (Lo and Zang, 2008) and also the Peaker parameter, used in VLF (Pedersen, 1998), the TPR grid imaging of geoelectric structures is omni-directional, with all orientations being highlighted. These results are compared against the pole-reduced (RTP) aeromagnetic image presented in Figure 10.

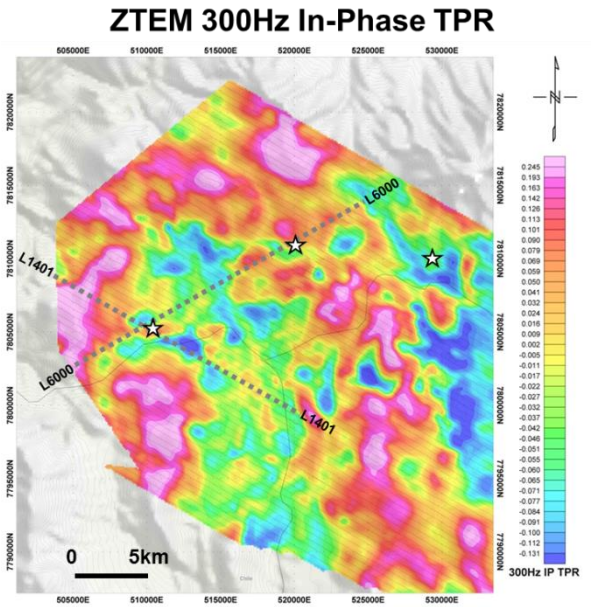

Figure 8: ZTEM 300 Hz In-phase Total Phase Rotation (TPR) tipper results, with locations of geothermal hot springs and also 2D ZTEM inversions shown in Figure 11 and Figure 13.

Whereas the higher frequency 300Hz IP TPR image in Figure 8 highlights the shallower geologic features that are mainly influenced/controlled by topography, the lower frequency 25Hz IP TPR in Figure 9 images the deeper, bedrock geology. This is highlighted using the structural geology overlay from Figure 4, which is also used in the magnetic image in Figure 10. Clearly the ZTEM resistivity

images are defining the same major features identified in the geology and the magnetics - with NE-SW and NW-SE, and also more NS structures; as well as others, including a prominent short strike-length NE-trending conductivity high feature that coincides with the known Lirima geothermal target area. This feature can also be followed as a narrow resistivity break further to the northeast to San Andrés, where a major resistivity contact is defined along the quebrada that coincides with a fault-contact between younger Pleistocene volcanics to the NW and older Miocene volcanic basement to the SE. A similar, but subtler, NW-SE oriented resistivity contact is also defined in the lower frequency TPR along the same type of Miocene-Pleistocene contact that controls the Chalviri hot springs structure. Several other prominent linear ZTEM conductive anomalies, similar to that found at Lirima, are also defined below the pampa overburden cover elsewhere in the Coscaya River Basin, further to the southeast (Figure 9).

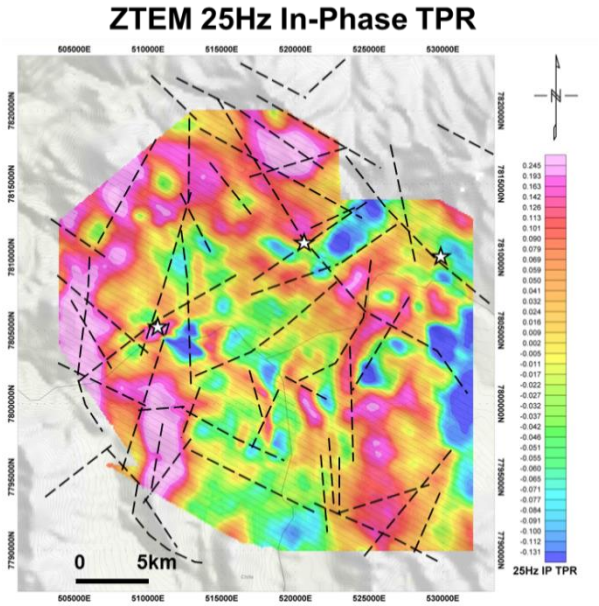

Figure 9: ZTEM25 Hz In-phase Total Phase Rotation (TPR) tipper results, with geologic structures from Figure 4.

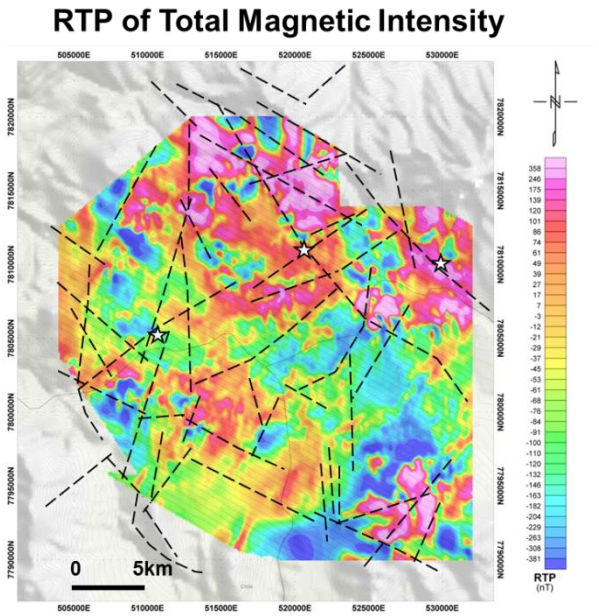

Figure 10: ZTEM aeromagnetic total magnetic intensity after reduction to pole (RTP), with structures from Figure 4.

ZTEM 2D INVERSION RESULTS

The ZTEM survey tipper results can be converted to their equivalent resistivity-depth source model using 2D inversion, as shown in Figure 11. The older Zvert2d algorithm (Legault et al., 2009) had been adapted for ZTEM by accounting for the air layer, as well as the mobile Hz and fixed Hx base station. The new Av2dtopo code (Legault et al., 2012), which now accounts for 2D ground topography, also uses the finite element forward problem and inversion parameter sensitivities using reciprocity of Wannamaker et al. (1987) and de Lugao and Wannamaker (1996), with the regularized Gauss-Newton non-linear parameter step estimate of Tarantola (1987). It also implements a depth-of-investigation (DOI) index (see Figure 11), using the 1.5x MT maximum skin depth and integrated 1D conductance method of Spies (1989).

The input data for the ZTEM 2D inversions were the In-line (Tzx) In-Phase and Quadrature Phase data from all six measured frequencies (25-600Hz). Based on previous ground resistivity results, a 100 ohm-metres half-space was used as the apriori starting model. Using an assigned data error of 1-2%, a convergence value of nRMS of close to unity (1.0) was achieved in 5 iterations for most lines at Pampa Lirima.

Figure 11 presents the ZTEM 2D inversion results for L1401, a NW-SE section directly across the Lirima geothermal field (see Figure 8) that roughly coincides with the NW-SE trending 3D MT section shown in Figure 7b. The 2D inversion for L6000, shown in Figure 12, represents a N-60OE oriented "virtual" tie-line that is orthogonal to L1401 and that was extracted from the in-line tipper vector data from adjacent ZTEM flight-lines. L6000 roughly coincides with the NE-SW trending 3D MT section presented in Figure 7a. Figure 13 presents a 500m depth-slice obtained from the 3D resistivity voxel created from the 2D ZTEM inversions at Pampa Lirima and highlighting the inferred NE-trending resistivity high lineament that corresponds with a similar 3D MT feature identified in Figure 7b.

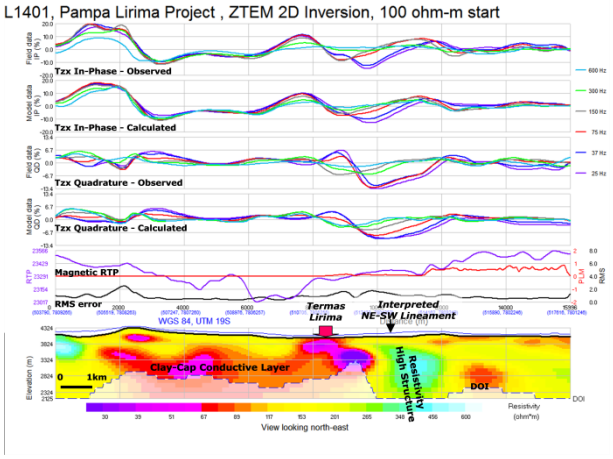

Figure 11: 2D ZTEM inversion for L1401 across the Lirima geothermal field that roughly coincides with the NW-SE trending 3D MT inversion section in Figure 7b.

Although skin depth DOI estimates suggest that the ZTEM does not image below 1.5-2km depths and therefore cannot corroborate the deep MT "intrusive" conductive

body, there is nevertheless good similarity between the 2D ZEM sections and the 3D MT model images, particularly the broad "clay-cap" conductive layer that extends west of Lirima - although it not as conductive and is also slightly deeper at ~1km depth in the ZTEM (vs. ~500m in 3D MT). Indeed, the Lirima and San Andrés hot spring both feature distinctive, localized, resistivity low anomalies in the ZTEM images (see Figure 11, Figure 12 & Figure 13), which are consistent with the previous TDEM and VES results, and likely relate to the stronger argillic alteration that is present. A deeper conductivity high is also observed at >500m depths in the L1401 ZTEM 2D image (Figure 11) just southeast of Lirima that might represent even stronger clay-alteration or fault-fracturing at depth. Finally, the inferred NE-trending high resistivity MT structure that bordered Lirima to the southeast also appears to be corroborated by a similar feature in the ZTEM 2D inversion results (see Figure 11 & Figure 13).

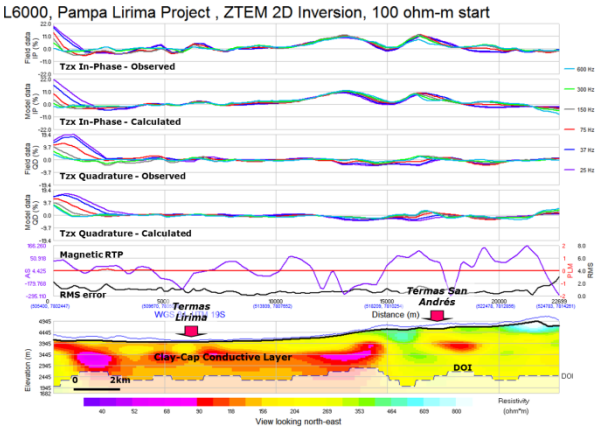

Figure 12: 2D ZTEM inversion for L6000, a "virtual" tie-line that crosses the Lirima geothermal field and roughly coincides with the NE-SW trending 3D MT inversion in Figure 7a.

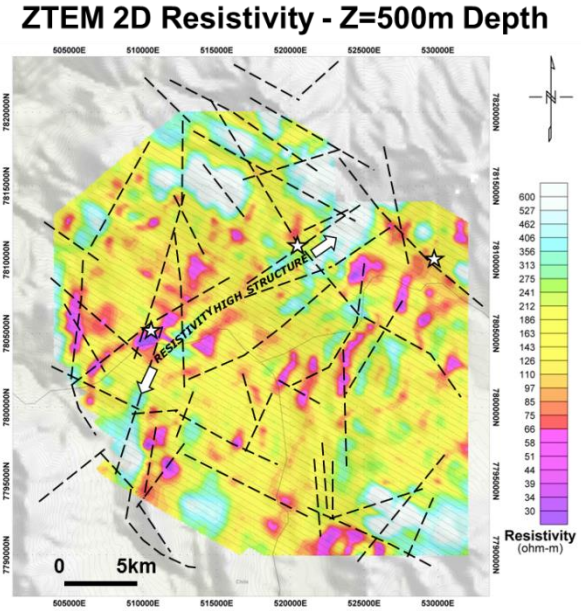

Figure 13: ZTEM resistivity-depth slice at 500m depth from 2D inversions, with structures from Figure 4, and inferred NE-trending resistivity high structure that corresponds with a similar 3D MT feature identified in Figure 7b.

CONCLUSIONS

The ZTEM results at Pampa Lirima appear to correlate well with previous geophysical results and the known geology, in particular the presence of major NE, NW and NS regional fault structures and geologic contacts. In addition, the ZTEM results define a prominent, localized, NE-trending conductivity high at Lirima hot springs that is consistent with stronger argillic alteration and VES and TDEM anomalies. It is also aligned along a more regional geologic lineament extending to the San Andrés hot springs 10km away. The San Andrés is associated with a major NE-trending ZTEM resistivity contact, however no distinctive conductivity high anomaly is observed similar to that found at Lirima – which also seems to be consistent with the previous geophysics. A nearly similar NW-SE geoelectric contact is observed in the ZTEM results at the Chalviri hot spring to the north east. Other conductivity highs like that observed at Lirima are visible below the overburden covered pampas further south east and represent logical targets for future follow-up.

The ZTEM airborne EM results and previous ground MT survey results at Pampa Lirima were compared using 2D and 3D inversions, respectively. Although, because of insufficient skin depth penetration (<1.5-2km), the ZTEM results were not able to corroborate a major deep MT conductivity high of interest at >2km depth below Pampa Lirima, the 2D ZTEM inversion images appear to agree very well with the MT, in-cluding the presence of a large-area "clay-cap" conductive layer at >500m-1km below the Lirima pampa valley. In addition to defining a conductivity anomaly over Lirima hot springs, a northeast trending horst-like MT resistivity high, east of Lirima, which coincides with an inferred NE-trending structural lineament, is also corroborated in the ZTEM inversion results, but whose impact on the conceptual geothermal system model is yet to be determined.

Additional 3D ZTEM and possibly joint ZTEM-MT inversions should improve the quality, depth-control and aerial extent of the resistivity characterization of the Pampa Lirima survey area, hopefully leading to the identification and characterization of other buried, undiscovered geothermal fields in the region.

ACKNOWLEDGEMENT

The authors thank Energía Andina for graciously allowing us to present these results. Our thanks to Kyle Orlowski for his assistance with preparing the figures and to GRC reviewer Patrick Dobson for his editorial comments.

REFERENCES

Arcos, R., J. Clavero, A. Giavelli, S. Simmons, I. Aguirre, S. Martini, C. Mayorga, G. Pineda, J. Parra, and J. Soffia, 2011, Surface exploration at Pampa Lirima geothermal project, Central Andes of Northern Chile, Geothermal Resources Council Transactions, 35, 689-693.

De Lugao, P.P., and P.E. Wannamaker, 1996, Calculating the two-dimensional magnetotelluric Jacobian in finite elements using reciprocity, Geophysical Journal International, 127, 806-810.

Geodatos, 2010, Estudio Geofisico transiente electromagnetico TEM y NanoTEM, Sector Pampa Lirima, Region de Tarapaca, Chile, Technical report for Energía Andina.

Haraldsson, I.G., 2012, Geothermal activity and developments in South America: A short overview of Bolivia, Chile, Co-lumbia, Ecuador, and Peru, a paper presented at "Short Course on Geothermal and Geothermal Wells", United Nations Uni-versity UNU-GTP Geothermal Training Programme, 18p.

Hermance, J. F., and R. E. Thayer, 1975, The telluric-magnetotelluric method: Geophysics, 37, 349–364.

Holtham, E., and D. Oldenburg, 2010, Three-dimensional inversion of ZTEM data, SEG Expanded Abstracts, 29, 655-659.

JICA, 1978, Infrastructural survey report for the development of the Cerro Colorado copper mine in the Republic of Chile, Japan International Cooperation Agency report, 199 p.

Labson, V.F., A. Becker, H.F. Morrison, and U. Conti, 1985, Geophysical exploration with audio frequency natural magnetic fields, Geophysics, 50, 656-664.

Lazaro, M., S. Alm, A. Tiedeman, C. Page, D. Meade, J. Shoffner, and K. Bucher, 2011, Department of the Navy Geo-thermal Exploration on Naval Air Station Fallon (NASF) Managed Lands in Dixie Valley, Nevada, Geothermal Re-sources Council Transactions, 35, 873-878.

Legault, J.M., H. Kumar, B. Milicevic, and P.E. Wannamaker, 2009, ZTEM tipper AFMAG and 2D Inversion results over an unconformity uranium target in northern Saskatchewan, SEG Expanded Abstracts, 28, 1277-1281.

Legault, J.M., J.B. Witter, P. Berardelli, and M. Orta, 2010, ZTEM airborne AFMAG EM results over the Reese River geothermal test area, central Nevada, 21ST ASEG International Geophysical Conference and Exhibition, Australian Society of Exploration Geophysicists, Extended Abstracts, 4p.

Legault, J.M., J.B. Witter, P. Berardelli, S. Lombardo, and M. Orta, 2011, Recent ZTEM airborne AFMAG EM survey re-sults over Reese River and other geothermal test areas, Geo-thermal Resources Council Transactions, 35, 879-884.

Legault, J.M., S. Zhao, and R. Fitch, 2012, ZTEM airborne AFMAG survey results over low sulphidation epithermal gold-silver vein systems at Gold Springs, south eastern Nevada, 22ND ASEG International Geophysical Conference and Exhibition, Australian Society of Exploration Geophysicists, Extended Abstracts, 4p.

Lo, B., and M. Zang, 2008, Numerical modeling of Z-TEM (airborne AFMAG) responses to guide exploration strategies, SEG Expanded Abstracts, 27, 1098-1101.

Mackie, R.L., and T.R. Madden, 1993, Three dimensional magnetotelluric inversion using conjugate gradients. Geophys-ical Journal International, 115, 215-229.

Pedersen, L.B., 1998, Tensor VLF measurements: Our first experiences, Exploration Geophysics, 29, 52-57.

Spies, B., 1989, Depth of investigation in electromagnetic sounding methods, Geophysics, 54, 872-888.

Stodt, J.A., G. W. Hohmann, and S. C. Ting, 1981, The telluric-magnetotelluric method in two- and three-dimensional environments: Geophysics, 46, 1137–1147.

Tarantola, A., 1987, Inverse Problem Theory, Elsevier, New York, 613 pp.

Vozoff, K., 1972, The magnetotelluric method in the explora-tion of sedimentary basins: Geophysics, 37, 98–141.

Wannamaker, P. E., J.A. Stodt, and L. Rijo, 1987, A stable finite element solution for two dimensional magnetotelluric modeling: Geophysical Journal of Royal Astronomical Society, 88, 277-296.

Ward, S. H., 1959, AFMAG - Airborne and Ground: Geo-physics, 24, 761-787